communications biology

A Nature Portfolio journal

Article

https://doi.org/10.1038/s42003-025-08116-6

USP22 enhances atherosclerotic plaque stability and macrophage efferocytosis by stabilizing PPARγ

Senhu Tang[1,2,4], Chuanghong Lu[1,2,4], Zhongyuan Meng[1,2,4], Zihua Ye[1,2], Yue Qin[1,2], Na Na[3], Shenglin Xian[1,2], Feng Huang[1,2] ✉ & Zhiyu Zeng[1,2] ✉

Atherosclerosis is a chronic inflammatory disease that strongly threatens human health, and macrophages play a pivotal role in its pathogenesis. Ubiquitin-specific peptidase 22 (USP22) is involved in the regulation of macrophage inflammation. However, its role in the atherosclerotic microenvironment remains unclear. In this study, we found that USP22 overexpression in macrophages alleviated atherosclerosis progression in ApoE$^{-/-}$ mice. In vitro, USP22 silencing enhanced macrophage inflammation and foam cell formation, and macrophage efferocytosis was significantly impaired. Mechanistically, USP22 bound to peroxisome proliferator-activated receptor γ (PPARγ) and inhibited its ubiquitination, thereby stabilizing PPARγ and promoting efferocytosis. In addition, intraperitoneal injection of the USP22 inhibitor USP22i-S02 exacerbated atherosclerosis in ApoE$^{-/-}$ mice. In summary, these findings indicate that USP22 may be a potential therapeutic target for the treatment of atherosclerosis.

Coronary artery disease caused by atherosclerosis is the leading cause of death worldwide, accounting for 32% (17.9 million) of deaths in 2019[1,2]. Atherosclerosis is a chronic progressive inflammatory disease primarily affecting medium and large arteries[3]. As key players in inflammation, macrophages are involved throughout all stages of atherogenesis and progression, from plaque formation to the transition to vulnerable plaques, making them as critical therapeutic targets for atherosclerosis. Previously, it was believed that macrophages are involved in atherogenesis, mainly through their phagocytosis of lipids, leading to excessive foam cell accumulation in the arterial wall[4,5]. However, increasing evidence has revealed various macrophage-induced atherosclerosis mechanisms, including impaired autophagy[6], decreased efferocytosis capacity[7] and M1 macrophage polarization[8]. Among them, efferocytosis plays a crucial role in atherosclerosis as a key mechanism for maintaining tissue homeostasis[9].

Efferocytosis refers to the process by which apoptotic cells are cleaned by specialized phagocytes such as macrophages as well as nonspecialized phagocytes (epithelial cells and smooth muscle cells). Efferocytosis consists of three phases: apoptotic cell recognition (discovery and binding), phagocytosis (internalization) and degradation. Both experimental and clinical studies have shown that efferocytosis is impaired in certain diseased tissues, including advanced atherosclerotic plaques[3,10–13]. Impaired macrophage efferocytosis is a key component of atherosclerotic plaque vulnerability. Therefore, there is an urgent clinical need to understand the key molecules regulating efferocytosis in atherosclerotic plaques. Previous findings suggest that the ubiquitinproteasome system is involved in the development of atherosclerosis[14,15]. Deubiquitination enzymes (DUBs) are proteases that cleave ubiquitin molecules from ubiquitin-linked substrates. In one study, ubiquitin-specific peptidase 9X (USP9X) was identified as a deubiquitinating enzyme that reduces lipid uptake in macrophages[16]. In addition, ubiquitin-specific peptidase 14 (USP14) in endothelial cells attenuates atherosclerosis by inhibiting nuclear factor-k-gene binding (NF-κB)[17]. However, the role of DUBs in efferocytosis is unknown.

Ubiquitin-specific peptidase 22 (USP22) belongs to the USP family of deubiquitinating enzymes and is predominantly localized in the cytoplasm and nucleus. USP22 has long been associated with a poor prognosis in cancer and neurological diseases[18,19]. To date, little is known about the role of USP22 in inflammatory diseases. It has been shown that USP22 protects cardiomyocytes from ischemia-reperfusion injury by inhibiting myocardial ferroptosis via the SIRT1/p53/SLC7A11 pathway[20]. USP22 in macrophages promotes LRR and PYD structural domain protein 3 (NLRP3) degradation and attenuates inflammation through autophagy-associated 5 homolog (ATG5)-mediated autophagy[21]. Furthermore, silencing USP22 in

[1]Department of Cardiology, The First Affiliated Hospital of Guangxi Medical University, Nanning, Guangxi, China. [2]Guangxi Key Laboratory of Precision Medicine in Cardio-Cerebrovascular Diseases Control and Prevention, Guangxi Clinical Research Center for Cardio-cerebrovascular Diseases, Nanning, Guangxi, China. [3]Department of Neuroscience, Scripps Research Institute, San Diego, CA, USA. [4]These authors contributed equally: Senhu Tang, Chuanghong Lu, Zhongyuan Meng. ✉e-mail: huangfeng@sr.gxmu.edu.cn; zengzhiyu@gxmu.edu.cn

macrophages promotes foam cell formation[16]. However, the role of USP22 in macrophages in atherosclerosis and whether it is associated with efferocytosis has not been elucidated. The inflammatory state of macrophages and increased lipid uptake impair efferocytosis[22–24]. Interestingly, USP22 plays an anti-inflammatory and inhibitory role in lipid uptake in macrophages[16,21], suggesting that USP22 may be an important molecule in the regulation of macrophage efferocytosis as well as a therapeutic target for atherosclerosis.

Here, we used ApoE$^{-/-}$ mice to establish a model of advanced atherosclerosis by feeding the mice a Western diet (WD). We found that USP22 overexpression in macrophages alleviated atherosclerosis in ApoE$^{-/-}$ mice. Unexpectedly, the antiatherosclerotic effect of USP22 was associated with increased efferocytosis through its ability to bind to peroxisome proliferator-activated receptor γ (PPARγ) and modulate PPARγ stability.

Results

Decreased USP22 expression in macrophages in severe atherosclerosis lesions

A previous study showed that USP22 deficiency in macrophages significantly promotes alum-induced peritoneal inflammation[21]. However, the role of USP22 in atherosclerosis is unclear. Eight-week-old ApoE$^{-/-}$ mice were fed a WD or chow diet for 16 weeks (Fig. 1A). We found that aortic tissue USP22 protein expression was lower in ApoE$^{-/-}$ mice fed a WD for 16 weeks than in ApoE$^{-/-}$ mice fed a chow diet for 16 weeks (Fig. 1B). Subsequent immunofluorescence staining analysis revealed that the average fluorescence intensity of USP22 protein in CD68^{+} macrophages within atherosclerotic lesion areas was lower in ApoE$^{-/-}$ mice fed a WD for 16 weeks compared to those fed a chow diet for 16 weeks (Fig. 1C). In addition, we treated THP-1-derived macrophages with LPS and IFN-γ for 24 h in vitro, and USP22 protein expression was also significantly decreased (Fig. 1D). Collectively, these results suggest that USP22 in macrophages may play an important role in the development of atherosclerosis.

Overexpression of USP22 in macrophages alleviates atherosclerosis in ApoE$^{-/-}$ mice

To explore the role of USP22 in macrophages in atherosclerosis, we constructed an animal model of USP22 overexpression in macrophages by injecting adeno-associated virus carrying the F4/80 promoter of macrophages and the flag-tagged USP22 gene (AAV-F4/80-OE-USP22) into 7-week-old male ApoE$^{-/-}$ mice and the AAV-empty vector was injected as a control. These ApoE$^{-/-}$ mice were fed a WD starting at 8 weeks of age and continuing for 16 weeks (Fig. 2A). Immunofluorescence staining of aortic sections revealed the colocalization of CD68 with Flag (Supplementary Fig. S1A), which suggested that AAV-F4/80-OE-USP22 could be

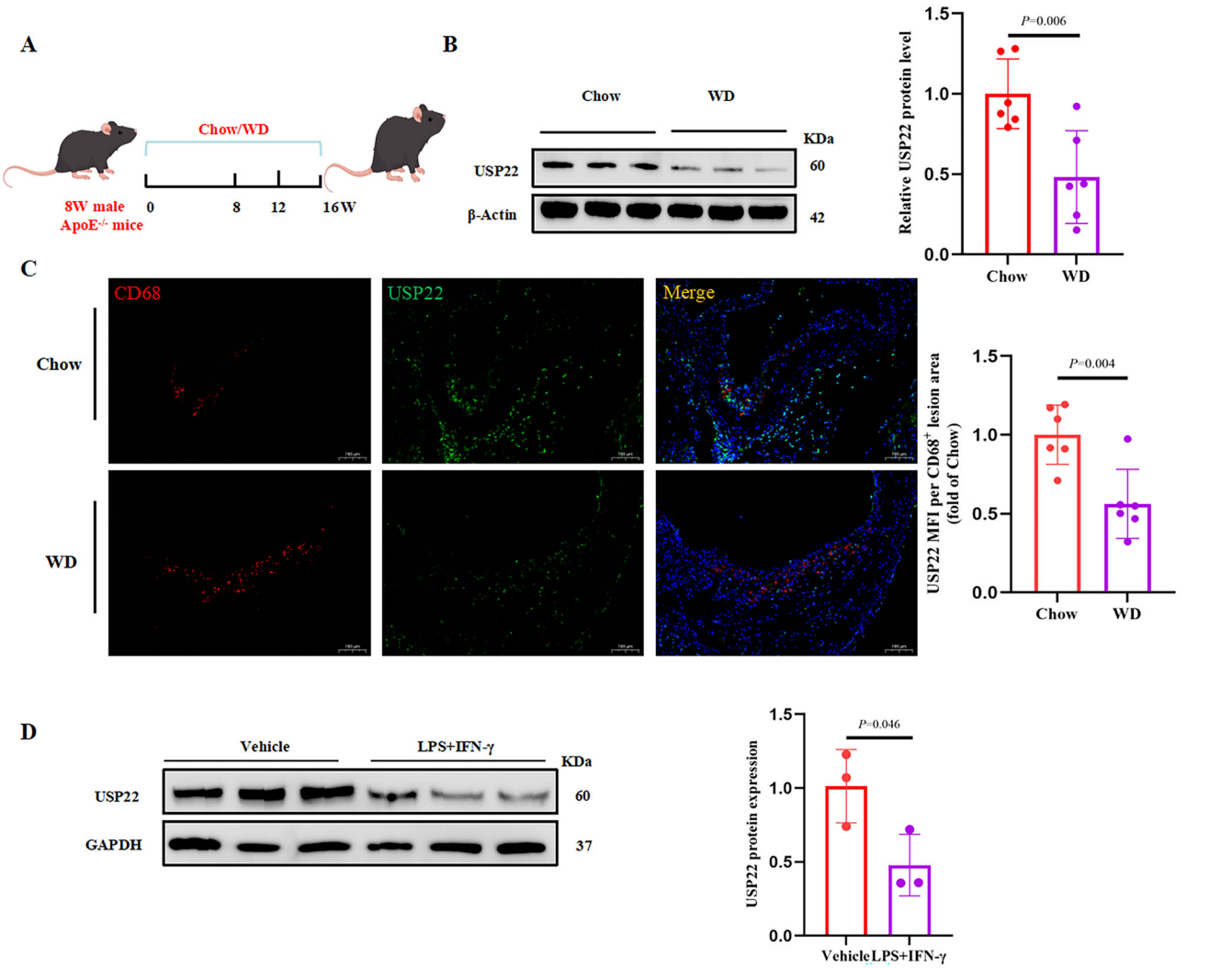

Fig. 1 | Decreased USP22 expression in macrophages in severe atherosclerosis lesions. A 8-week-old ApoE$^{-/-}$ mice were fed a WD or chow diet for 16 weeks. **B** Protein levels were measured by western blot ($n = 6$). **C** Sections of the aortic sinus from ApoE$^{-/-}$ mice were co-stained with USP22 (green), CD68 (red) and nuclei (DAPI, blue). USP22 staining was quantified as the MFI within CD68^{+} macrophages ($n = 6$). Scale bar: 100 μm. **D** Representative gel images and quantification of USP22 in THP-1-derived macrophages are shown, and GAPDH was used as a control ($n = 3$). *P* values are shown in the figure. Two-tailed unpaired *t*-test (**B**–**D**).

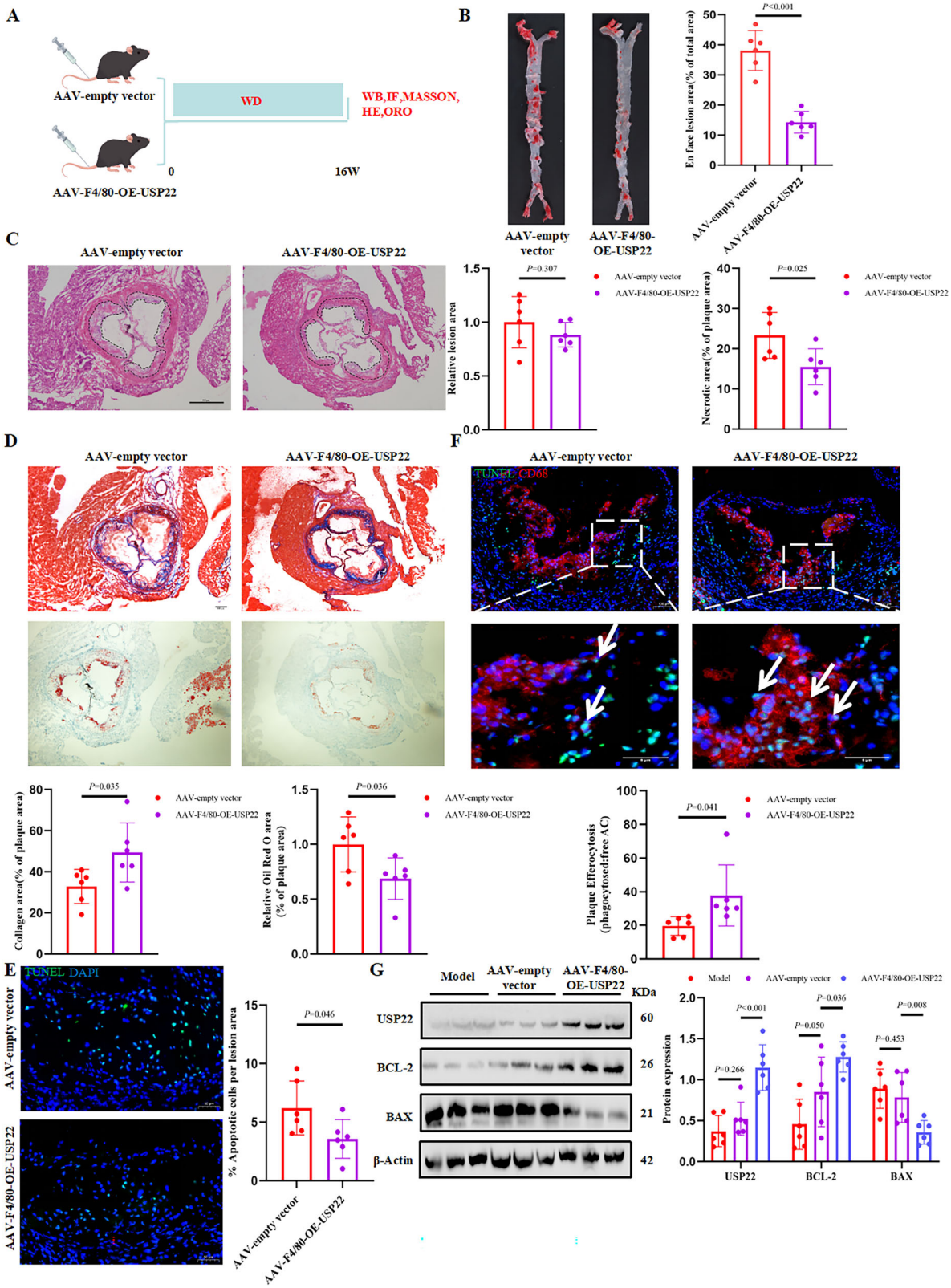

Fig. 2 | Overexpression of USP22 in macrophages by AAV in WD-fed ApoE$^{-/-}$ mice results in smaller plaque necrotic core areas and improves efferocytosis in atherosclerotic plaques. **A** In vivo experimental timeline. **B** ApoE$^{-/-}$ mice were subjected to ORO staining of aorta. **C** Representative images and quantification of H&E-stained aortic sinus cross-sectional sections are shown. The plaque area is marked (dashed line). Scale bar: 500 μm. **D** Representative images and quantification of Masson and ORO staining of aortic sinus cross-sectional sections are shown. Scale bar: 200 μm. **E** Sections of the aortic sinus were co-stained with TUNEL (green) and nuclei (DAPI, blue). Scale bar: 50 μm. **F** Representative fluorescent images and quantification of lesion efferocytosis are shown. Scale bar: 100 μm. The white arrows represent macrophage-associated apoptotic cells, and the boxed areas are magnified. Scale bar: 5 μm. **G** Protein levels were measured by western blot, model group represents ApoE$^{-/-}$ mice fed WD for 16 weeks. Each point is from a single mouse. *P* values are shown in the figure. Two-tailed unpaired *t*-test (**B**–**F**). One-way ANOVA (**G**). ($n = 6$).

successfully translocated into macrophages. In addition, western blot assay also confirmed this finding (Fig. 2G). Compared with those of the controls, the percentages of the plaque necrotic area and Oil red O (ORO)-positive area were decreased (Fig. 2B–D), and the percentage of the collagen content was increased (Fig. 2D) in ApoE$^{-/-}$ mice with USP22-overexpressing macrophages. However, no significant change in lesion area was observed between the two groups (Fig. 2C). We also found that ApoE$^{-/-}$ mice with USP22-overexpressing macrophages had a lower percentage of macrophages in plaques as well as lower plasma interleukin-1β (IL-1β) and monocyte chemoattractant protein-1 (MCP-1) levels than controls did (Supplementary Fig. S1B, Table S1). Body weight, low-density lipoprotein cholesterol (LDL-C), and high-density lipoprotein cholesterol (HDL-C) levels were comparable between the two groups of mice (Supplementary Table S1).

It is well known that prolonged accumulation of foam cells leads to apoptosis, and if they are not cleared by efferocytosis, they become necrotic and exacerbate inflammation. Therefore, we explored whether the overexpression of USP22 in macrophages affects the accumulation of apoptotic cells. We observed that the percentage of apoptotic cells within lesions was lower in ApoE$^{-/-}$ mice in which USP22 was overexpressed in macrophages than in control mice (Fig. 2E). Because the decrease in the number of apoptotic cells within lesions can be caused by either decreased apoptosis or increased efferocytosis, we next determined whether the overexpression of USP22 in macrophages affects macrophage efferocytosis. The results revealed that the ratio of macrophage-associated TUNEL-positive cells to free TUNEL-positive cells was greater in the lesions of ApoE$^{-/-}$ mice with USP22 overexpression in macrophages than in those of controls (Fig. 2F), which indicated that USP22 enhanced efferocytosis, and these results were consistent with the smaller necrotic core area found in the aortas of ApoE$^{-/-}$ mice with USP22 overexpression in macrophages (Fig. 2C). We subsequently demonstrated decreased BCL2-associated X (BAX) protein expression and elevated B-cell lymphoma-2 (BCL-2) protein expression in the aortic tissues of ApoE$^{-/-}$ mice with USP22 overexpression in macrophages compared with those of controls (Fig. 2G). These results suggest that overexpression of USP22 in macrophages alleviates the progression of atherosclerosis in mice by inhibiting lipid deposition and enhancing efferocytosis.

Overexpression of USP22 in macrophages inhibits foam cell formation, inflammation, and macrophage apoptosis

Because overexpression of USP22 in macrophages did not reduce lipid levels in ApoE$^{-/-}$ mice, we hypothesized that the reduced lipid deposition in the lesions of ApoE$^{-/-}$ mice with USP22 overexpression in macrophages might be caused by reduced lipid uptake by macrophages. We used human Si-USP22-1/2/3 and Si-Ctrl to transfect THP-1-derived macrophages for 48 h. Western blot analysis verified that USP22 was significantly inhibited by Si-USP22-1 (Fig. 3A, Supplementary Fig. S1C); thus, all subsequent related experiments were performed with Si-USP22-1. In addition, we also used siRNA transfection of bone marrow-derived macrophages (BMDMs) as well as lentiviral infection of THP-1 cells to stably overexpress USP22 (Fig. 3A). We subsequently demonstrated that silencing USP22 enhanced lipid uptake and foam cell formation, whereas overexpressing USP22 inhibited lipid uptake and foam cell formation (Fig. 3B–D). To elucidate the molecular mechanisms by which USP22 regulates lipid uptake. We examined the protein expression of cluster of differentiation 36 (CD36), recombinant macrophage scavenger receptor 1 (MSR1) and lectin-like oxidized low density lipoprotein receptor 1 (LOX-1), the major lipid uptake molecules in macrophages, by western blot assay. The results revealed that overexpression of USP22 resulted in a statistically significant decrease in CD36 and LOX-1 in macrophages, that of MSR1 was mildly elevated but not statistically significant, and that silencing of USP22 resulted in a statistically significant increase in CD36 and LOX-1 (Supplementary Fig. S2). In conclusion, USP22 inhibits lipid uptake and reduces foam cell formation probably by decreasing CD36 and LOX-1 expression. Next, we also found that LPS and IFN-γ reduced USP22 protein expression in macrophages in a time-dependent manner. However, interleukin-4 (IL-4) and interleukin-13 (IL-13) increased USP22 protein expression in macrophages (Fig. 3E and F). In addition, we stimulated THP-1-derived macrophages with LPS and IFN-γ to model inflammatory macrophages. We observed reduced mRNA expression levels of MCP-1 and interleukin-12 (IL-12) and increased mRNA expression levels of the anti-inflammatory factors interleukin-10 (IL-10) and transforming growth factor-β (TGF-β) in THP-1-derived macrophages overexpressing USP22 compared with those in the control group (Fig. 3G). Finally, we observed that USP22 inhibited macrophage early apoptosis under basal and inflammatory conditions (Fig. 3H–J). Collectively, these results suggest that USP22 in macrophages inhibits foam cell formation, inflammation, and macrophage apoptosis.

USP22 in macrophages enhances efferocytosis

We observed in vivo that overexpression of USP22 in macrophages enhanced efferocytosis. Next, we investigated the effect of USP22 in macrophages on efferocytosis and the potential mechanism in vitro. We treated Jurkat cells with H_2O_2 to generate apoptotic jurkat cells (ACs), and the apoptosis rate of the Jurkat cells was >80%, as detected by flow cytometry (Supplementary Fig. S3A). We subsequently cocultured ACs with THP-1-derived macrophages for 2 h and detected increased USP22 protein expression in the macrophages (Fig. 4A). The increased USP22 expression in THP-1-derived macrophages could be caused by the phagocytosis of ACs or apoptotic cell conditioned medium (ACCM). We subsequently treated THP-1-derived macrophages with 10 μM cytochalasin D (CytD) for 30 min before they were cocultured with ACs, and CytD blocked internalization by inhibiting actin polymerization. We found that USP22 expression remained high in CytD-treated THP-1-derived macrophages compared with that in control cells not treated with CytD, which suggested that elevated expression of USP22 was not associated with internalization (Supplementary Fig. S3B). Furthermore, we learned that the increased USP22 protein expression in macrophages was due mainly to ACCM stimulation (Supplementary Fig. S3B).

Next, we explored the effect of USP22 on macrophage efferocytosis. We performed GSEA on the differential expression of transcripts (Supplementary data 1), which suggested that USP22 may promote efferocytosis (Supplementary Fig. S3C). We subsequently silenced USP22 in vitro, which showed impaired efferocytosis in THP-1-derived macrophages (Fig. 4B), and this finding was further confirmed by flow cytometry result (Fig. 4C). In addition, to determine the mechanism by which silencing USP22 inhibits efferocytosis, we used CytD to inhibit actin polymerization in THP-1-derived macrophages, which prevented the internalization of ACs. Any difference in the association of macrophages with ACs may be due to differences in the binding capacity of macrophages to ACs. As expected, compared with THP-1-derived macrophages transfected with Si-Ctrl, THP-1-derived macrophages transfected with Si-USP22 presented significantly decreased binding to ACs (Fig. 4C, Supplementary Fig. S3D). Therefore, we hypothesized that silencing USP22 might affect the expression of efferocytosis-associated receptors or bridging molecules, and further experiments revealed that USP22 silencing in macrophages resulted in a decrease in the expression of the efferocytosis-associated molecules anexelekto(AXL), c-mer proto-oncogene tyrosine kinase (MERTK), and milk fat globule epidermal growth factor 8 (MFG-E8), whereas no significant changes were observed in CD36 (Fig. 4D, E). In addition, the phagocytosis of fluorescent polystyrene beads by USP22-overexpressing THP-1-derived macrophages was greater than that in the control group (Fig. 4F). Finally, we used BMDMs to validate the effect of USP22 on efferocytosis, and the results were consistent with those observed in THP-1-derived macrophages (Fig. 4G–J, Supplementary Fig. S3D). These data suggest that USP22 affects efferocytosis by regulating the expression of efferocytosis-associated receptors or bridging molecules.

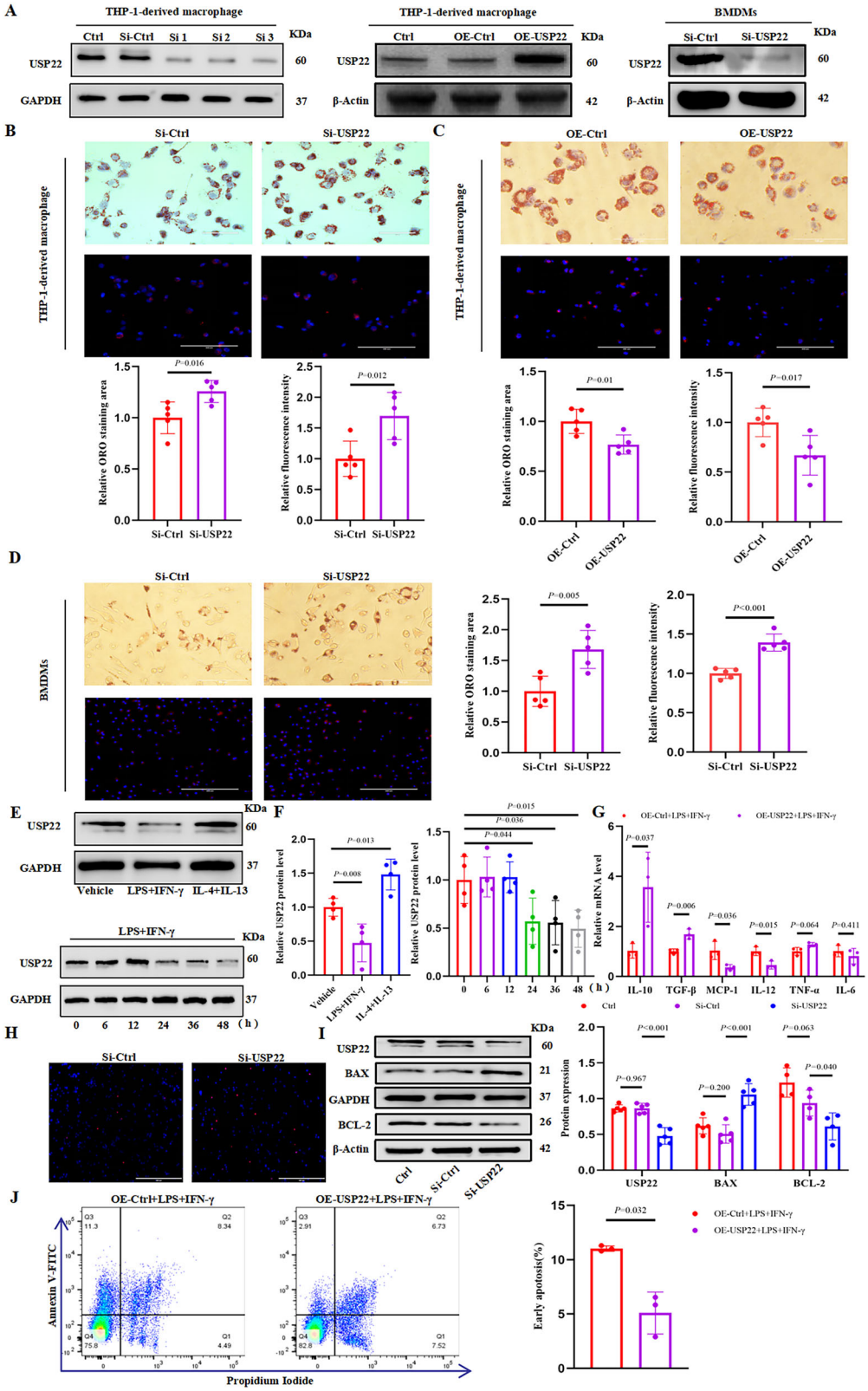

USP22 in macrophages regulates efferocytosis by stabilizing PPARγ

Previous studies have shown that PPARγ regulates macrophage inflammation, lipid metabolism, and the expression of efferocytosis-associated receptors[25–29]. In addition, USP22 has been found to stabilize PPARγ in hepatocellular carcinoma cells[30]. However, the relationship between USP22 and PPARγ in macrophages is unclear. We next investigated whether USP22 enhances efferocytosis by regulating PPARγ.

Interestingly, we found that USP22 may activate the PPAR signaling pathway in THP-1-derived macrophages (Fig. 4K, Supplementary data 1). PPARγ protein expression was upregulated in THP-1-derived macrophages and BMDMs treated with ACCM. However,

Fig. 3 | Downregulation of USP22 in macrophages promotes foam cell formation, inflammation and apoptosis. A Protein levels were measured by western blot. **B**, **C** Representative images and quantification of ORO staining and Dil-ox-LDL uptake in THP-1-derived macrophages are shown. ($n = 5$). Scale bar: 100 μm or 200 μm. **D** Representative images and quantification of ORO staining and Dil-ox-LDL uptake in BMDMs are shown ($n = 5$). Scale bar: 100 μm or 200 μm. **E, F** THP-1-derived macrophages were treated with LPS (100 ng/mL) and IFN-γ (20 ng/mL) or IL-4 (20 ng/mL) and IL-13 (20 ng/mL). Protein levels were measured by western blot ($n = 4$). **G** THP-1-derived macrophages were treated with LPS (100 ng/mL) and IFN-γ (20 ng/mL) for 24 h. RT-qPCR was performed to detect the mRNA levels of IL-10, TGF-β, MCP-1, IL-12, TNF-α, and IL-6 in THP-1-derived macrophages. ($n = 3$). **H** TUNEL staining in THP-1-derived macrophages is shown. Scale bar: 400 μm. **I** Protein levels were measured by western blot ($n = 4$–5). **J** THP-1-derived macrophages were treated with LPS (100 ng/mL) and IFN-γ (20 ng/mL) for 24 h. Representative images and quantification of early apoptotic cells are shown ($n = 3$). The n value represents the number of an individual cell culture well biological replicates. P values are shown in the figure. Two-tailed unpaired t-test (**B**, **C**, **D**, **G**, **J**). One-way ANOVA (**F**, **I**).

USP22 silencing in THP-1-derived macrophages and BMDMs resulted in decreased PPARγ protein expression (Fig. 5A). Given that USP22 is a deubiquitinating enzyme and that USP22 and PPARγ are localized mainly in the nucleus, we hypothesized that USP22 may regulate the expression of efferocytosis-associated receptors or bridging molecules by stabilizing PPARγ in the nucleus of macrophages. To test this hypothesis, we performed cytoplasmic and nuclear protein separation experiments and found that the protein expression of USP22 and PPARγ in the nucleus of THP-1-derived macrophages was elevated after ACCM stimulation. However, no significant changes in the cytoplasmic USP22 or PPARγ were detected (Fig. 5B). More importantly, we also found that silencing USP22 in THP-1-derived macrophages significantly decreased PPARγ protein expression in the nucleus (Supplementary Fig. S3E). However, inhibiting PPARγ in THP-1-derived macrophages with GW9662 did not affect USP22 protein expression (Fig. 5C). This suggested that PPARγ is a downstream factor of USP22. In addition, USP22 and PPARγ were colocalized mainly in the nucleus of THP-1-derived macrophages and BMDMs (Fig. 5D). We subsequently performed coimmunoprecipitation experiments to confirm the interaction between USP22 and PPARγ (Fig. 5E), and predicted their possible binding sites via HDOCK software (Fig. 5E). Next, we examined PPARγ protein levels in the presence of cycloheximide (CHX), a protein synthesis inhibitor. Notably, USP22 silencing in THP-1-derived macrophages resulted in a significant decrease in PPARγ protein stability (Fig. 5F). Thus, these results suggest that USP22 increases the stability of the PPARγ protein by binding to PPARγ in the nucleus of macrophages. To determine the mechanism of PPARγ reduction, we used the protease inhibitor MG132 to intervene in THP-1-derived macrophages, and the protein reduction in PPARγ caused by Si-USP22 was blocked by MG132 (Fig. 5G). Furthermore, USP22 significantly promoted PPARγ deubiquitination (Supplementary Fig. S4). These results suggest that silencing USP22 in THP-1-derived macrophages induces ubiquitinproteasome system-mediated degradation of the PPARγ.

Finally, we tested whether the decrease in PPARγ might be one of the molecular mechanisms by which USP22 silencing inhibits efferocytosis. Our results showed that the PPARγ agonist rosiglitazone reversed the decrease in macrophage efferocytosis caused by USP22 silencing (Fig. 5H–J, Supplementary Fig. S5A, B. Furthermore, for THP-1-derived macrophages under inflammatory conditions, USP22 overexpression also promoted efferocytosis. However, this effect was reversed by the PPARγ inhibitor GW9662 (Fig. 5K). Collectively, USP22 in macrophages promotes PPARγ stability and its mediated efferocytosis by binding PPARγ.

GW9662 reduces protective effect of USP22 overexpression in macrophages on atherosclerosis

To determine in vivo whether PPARγ may be an important downstream molecule of USP22 in the regulation of macrophage efferocytosis during atherosclerosis, we fed ApoE$^{-/-}$ mice injected with AAV-F4/80-OE-USP22 at 8 weeks of age a WD for 16 weeks, in which the latter 8 weeks were concomitantly injected intraperitoneally with GW9662 (1 mg/kg) every 3 days/dose (Fig. 6A). GW9662 significantly reduced PPARγ protein expression in aortic tissue (Fig. 6G). Compared with those in ApoE$^{-/-}$ mice injected with AAV-F4/80-OE-USP22 alone, the aortic root lesion area and the percentage of plaque necrotic core area increased in ApoE$^{-/-}$ mice given both GW9662 and AAV-F4/80-OE-USP22 (Fig. 6B), which was accompanied by increased lipid deposition (Fig. 6C and E) and increased plasma MCP-1 and IL-1β levels (Supplementary Table S2). However, no significant change in the percentage of plaque collagen content was observed between the two groups of mice (Fig. 6D). Body weight, HDL-C, and LDL-C levels were comparable between the two groups of ApoE$^{-/-}$ mice (Supplementary Table S2). We subsequently determined whether GW9662 influenced the promotion of efferocytosis by USP22 overexpression in macrophages in vivo. The results revealed that the ratio of macrophage-associated TUNEL-positive cells to free TUNEL-positive cells was lower in the lesions of ApoE$^{-/-}$ mice given GW9662 than in those of ApoE$^{-/-}$ mice injected with AAV-F4/80-OE-USP22 alone (Fig. 6F), which suggested attenuated efferocytosis.

Furthermore, we demonstrated that GW9662 reversed the increased expression of efferocytosis-associated receptors or bridging molecules in aortic tissues caused by the overexpression of USP22 in macrophages (Fig. 6G). Collectively, these results suggest that the protective effect of USP22 overexpression in macrophages against atherosclerosis is weakened by the PPARγ antagonist GW9662.

The USP22 inhibitor USP22i-S02 exacerbates atherosclerosis in ApoE$^{-/-}$ mice

Next, we determined the effect of USP22i-S02 on atherosclerosis in ApoE$^{-/-}$ mice in vivo. We divided ApoE$^{-/-}$ mice into 3 groups: (I) vehicle; (II) low-dose USP22i-S02 (L-USP22i-S02) (7.5 mg/kg); and (III) high-dose USP22i-S02 (H-USP22i-S02) (15 mg/kg). All mice were fed a WD for 16 weeks, with USP22i-S02 or vehicle intervention only during the last 8 weeks. USP22i-S02 or vehicle was treated by intraperitoneal injection every 3 days/dose. Body weight, HDL-C, and LDL-C were comparable in all groups of ApoE$^{-/-}$ mice (Supplementary Table S3). Interestingly, compared with those in the vehicle group, the percentages of plaque necrotic core areas and ORO-positive areas were greater in the aortic root lesions of ApoE$^{-/-}$ mice injected with high doses of USP22i-S02 (Fig. 7A, B). However, the percentage of plaque collagen content did not significantly differ among the three groups of mice (Fig. 7C). We also examined the plasma MCP-1 and IL-1β levels in these groups of mice, and the results showed that ApoE$^{-/-}$ mice injected with high doses of USP22i-S02 had significantly increased plasma MCP-1 and IL-1β levels compared with those in the vehicle group (Fig. 7D). These results suggest that USP22i-S02 aggravates atherosclerosis in ApoE$^{-/-}$ mice.

Discussion

Impaired macrophage efferocytosis is a major driver of atherosclerotic necrotic core formation[9,31]. Although numerous studies have revealed the mechanisms by which phagocytes recognize and take up apoptotic cells and the role of efferocytosis in avoiding inflammation over the past three decades[32–35], the endogenous regulatory pathways of efferocytosis remain incompletely defined. The present study reveals a novel association between the USP22-PPARγ signaling pathway and apoptotic cell clearance in macrophages, suggesting that USP22 may ameliorate atherosclerosis and enhance plaque stability through this mechanism.

In recent years, an increasing number of studies have shown that USP22 plays a key role in various cancers[36,37], revealing its great potential as a potential therapeutic target. However, the role of USP22 in inflammatory diseases has not been elucidated. In our study, USP22 expression was

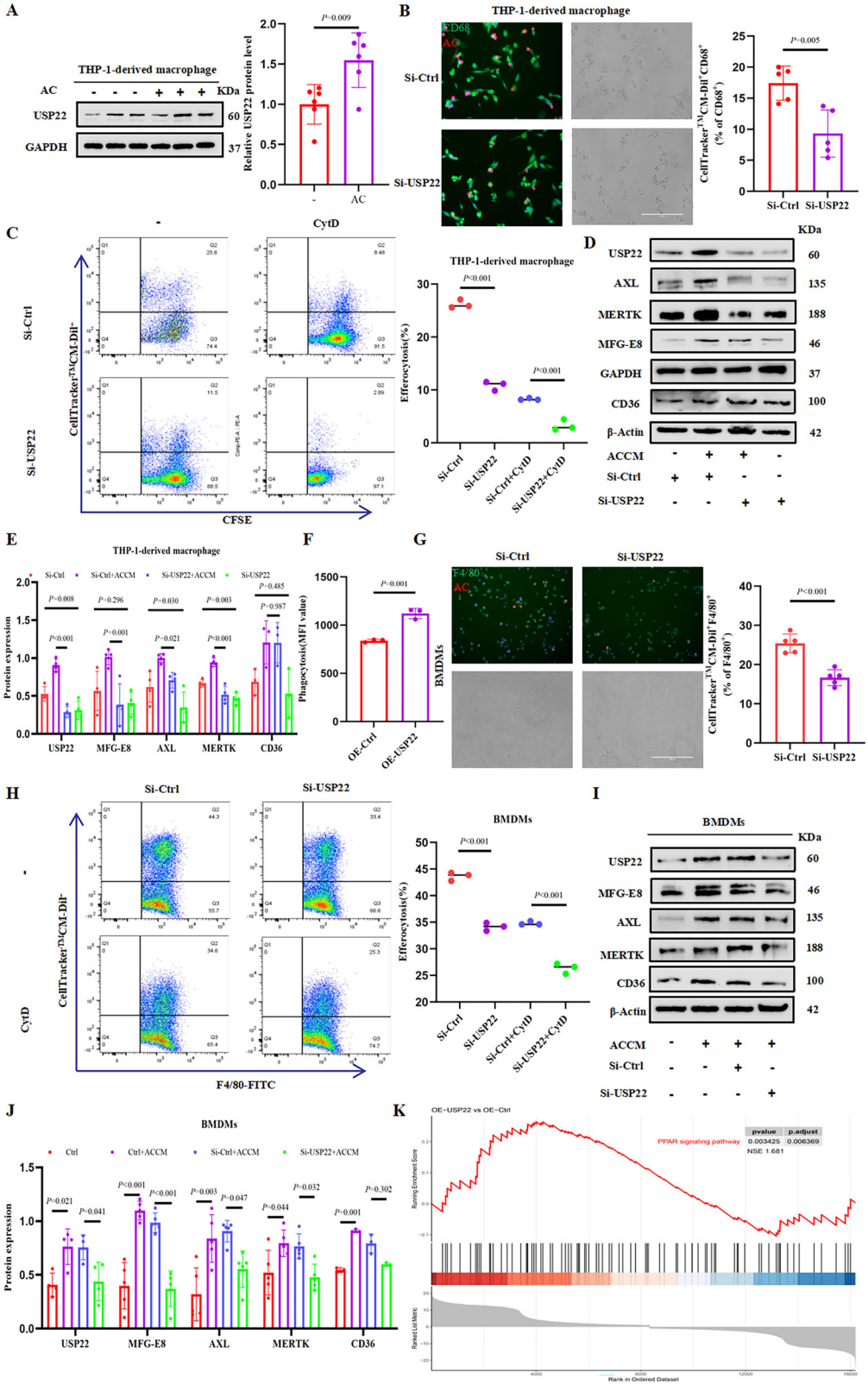

Fig. 4 | Downregulation of USP22 in macrophages inhibits efferocytosis. **A** Protein levels were measured by western blot ($n = 6$). **B** Representative images and quantification of efferocytosis in THP-1-derived macrophages are shown ($n = 5$). Scale bar: 200 μm. **C** Efferocytosis capacities of THP-1-derived macrophages detected by flow cytometry are shown ($n = 3$). **D**, **E** Protein levels were measured by western blot ($n = 3$–4). **F** Quantification of fluorescent polystyrene beads phagocytosed by THP-1-derived macrophages is shown ($n = 3$). **G** Representative images and quantification of efferocytosis in BMDMs are shown ($n = 5$). Scale bar: 200 μm. **H** Efferocytosis capacities of BMDMs detected by flow cytometry are shown ($n = 3$). **I**, **J** Protein levels were measured by western blot ($n = 3$–5). **K** Visualization of the GSEA result. The n value represents the number of an individual cell culture well biological replicates. P-values are shown in the figure. Two-tailed unpaired t-test (**A**, **B**, **F**, **G**). One-way ANOVA (**J**). Two-way ANOVA (**C**, **E**, **H**).

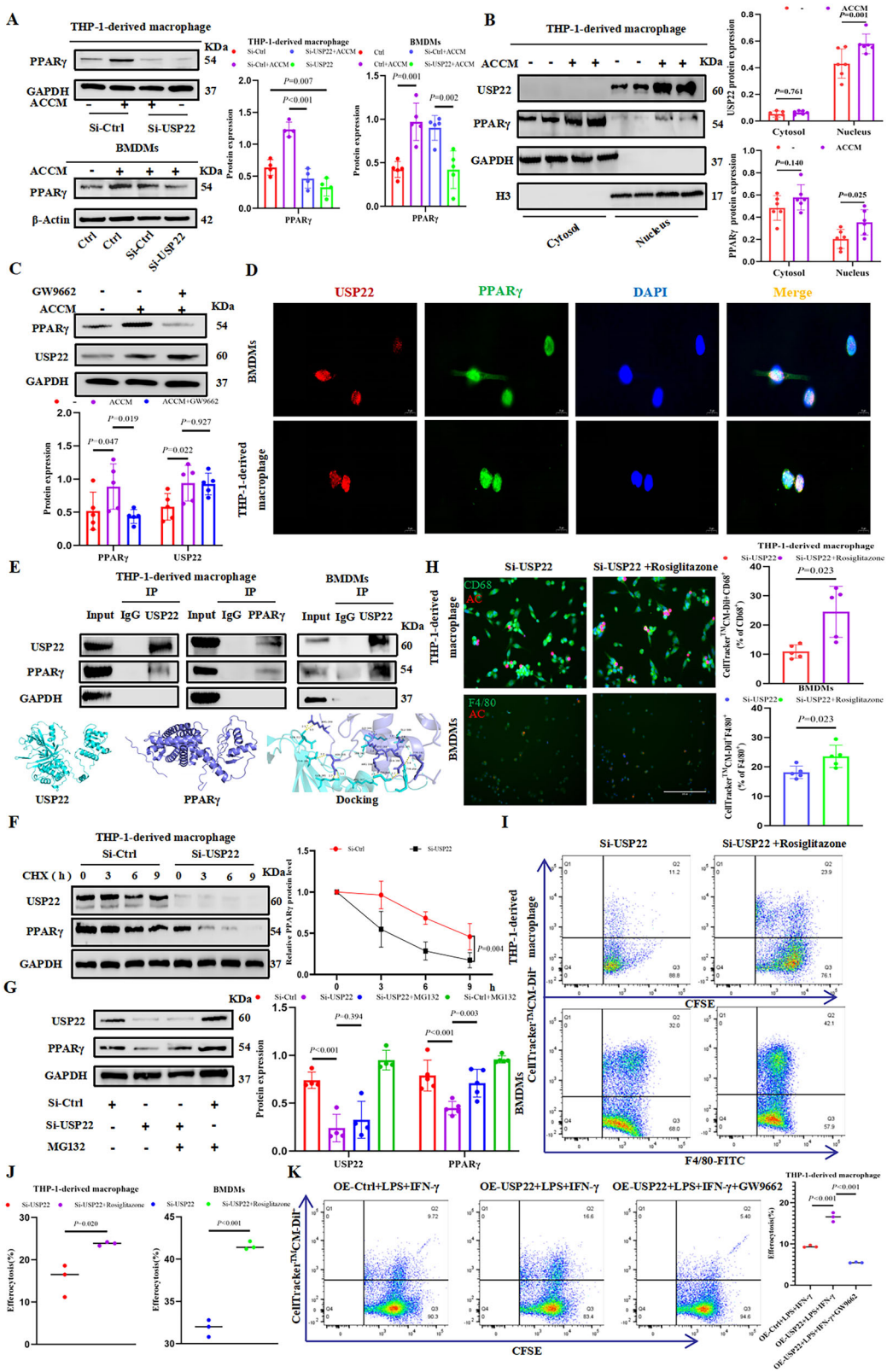

downregulated in macrophages or monocytes during atherosclerosis in humans and mice. In addition, we stimulated THP-1-derived macrophages with LPS and IFN-γ in vitro for 24 or 48 h, and USP22 protein expression was significantly decreased. Previously, LPS stimulation for 8 or 16 h was reported to result in a seemingly unchanged total USP22 protein levels in macrophages, with nuclear USP22 translocating to the cytoplasm and inhibiting inflammation through autophagy[21]. Thus, we infer that the possible mechanism is that in the early stage of inflammation, USP22 reduces the level of cellular inflammation through compensatory cytoplasmic translocation, and when the inflammatory stimulus is prolonged, USP22 is in a state of loss of compensation, its expression decreases markedly, and the cell undergoes a strong inflammation. Given that

Fig. 5 | USP22 in macrophages enhances efferocytosis by stabilizing PPARγ. **A** Protein levels were measured by western blot ($n = 4–5$). **B** Western blot analysis of USP22 and PPARγ in the cytosol and nucleus of THP-1-derived macrophages are shown. H3 was used as a nucleus control and GAPDH was used as a cytosol control ($n = 6$). **C** THP-1-derived macrophages were treated with 10 μM GW9662 for 24 h. Protein levels were measured by western blot ($n = 5$). **D** Triple immunofluorescence (IF) staining of USP22 (red), PPARγ (green) and nuclei (DAPI, blue) was performed in THP-1-derived macrophages or BMDMs. Scale bar: 10 μm. **E** Co-IP experiments were performed in THP-1-derived macrophages or BMDMs lysates. Proteins were measured by western blot ($n = 3$). The possible binding sites of USP22 and PPARγ predicted by HDOCK software are shown. **F** THP-1-derived macrophages were treated with 40 μM CHX. Stability analyses of the PPARγ protein in THP-1-derived macrophages transfected with Si-Ctrl or Si-USP22 are shown ($n = 4$). **G** THP-1-derived macrophages were treated with 10 μM MG132 for 6 h. Protein levels were measured by western blot ($n = 4–5$). **H** THP-1-derived macrophages or BMDMs were treated with 50 μM rosiglitazone for 24 h. Fluorescence images of macrophages (green) and apoptotic Jurkat cells (red) are shown ($n = 5$). Scale bar: 200 μm. **I**, **J** THP-1-derived macrophages or BMDMs were treated with 50 μM rosiglitazone for 24 h. Flow cytometry was performed to detect the efferocytosis of THP-1-derived macrophages or BMDMs ($n = 3$). **K** THP-1-derived macrophages were treated with 10 μM GW9662 for 24 h. Flow cytometry was performed to detect the efferocytosis of THP-1-derived macrophages under inflammatory conditions ($n = 3$). The *n* value represents the number of an individual cell culture well biological replicates. *P*-values are shown in the figure. Two-tailed unpaired *t*-test (**H**, **J**). One-way ANOVA (**A**, **C**, **K**). Two-way ANOVA (**A**, **B**, **F**, **G**).

inflammatory cytokines contribute to atherogenesis[38,39], We measured the levels of cytokine, including MCP-1, IL-12, IL-10, and TGF-β, and we subsequently reported that the overexpression of USP22 in macrophages both in vivo and ex vivo reduced the levesl of inflammatory factor. Similarly, Karlowitz et al. reported that USP22-deficient human intestinal epithelial cells significantly upregulate genes involved in interferon signaling and viral defense[40]. In addition, USP22-deficient hematopoietic stem progenitor cells exhibit increased expression of inflammation-related genes[41]. However, another study has shown that USP22 is highly expressed and localized to the nucleus in calcified human aortic smooth muscle cells and that USP22 promotes high-phosphorus-induced vascular calcification through activation of the NF-κB signaling pathway[42]. USP22 deletion diminishes the suppression of Treg cells without promoting broad inflammation[43]. Thus, we believe that USP22 has different effects on inflammation in different cells. Our results also suggest that the anti-atherogenic effect of USP22 is not due to alterations in the plasma lipid profile, but rather that USP22 inhibits lipid uptake by macrophages, which is consistent with the previously reported result[16]. In contrast, other studies have shown that USP22 promotes fatty acid synthesis in hepatocellular carcinoma cells and, thus, hepatocellular carcinoma progression[30]. The different effects of USP22 on cellular lipid metabolism may be related to factors such as the different cells studied and the disease microenvironment. In the context of neoplastic and inflammatory diseases, the function of USP22 may show diametrically opposite trends, a phenomenon that deserves our in-depth attention and exploration. In addition, since we observed in vivo that overexpression of USP22 in macrophages reduced the accumulation of apoptotic cells in plaques and that our in vitro experiments also revealed that USP22 reduced macrophage apoptosis under both basal and inflammatory conditions. However, the exact mechanism of action is still unclear, as previous studies have suggested that USP22 may be involved in cell cycle regulation and apoptosis through the deubiquitination of Cyclin D1 and SIRT1[44,45].

Defective efferocytosis leads to secondary necrosis of uncleared apoptotic cells, which exacerbates inflammation within the plaque. We unexpectedly found that USP22 in macrophages enhanced efferocytosis both in vitro and in vivo. Although USP22 overexpression had little effect on the plaque lesion area, it significantly reduced the plaque necrotic core area and increased the degree of plaque collagen deposition, which stabilized the plaques. However, in contrast, it has been demonstrated that USP22 deletion enhances bacterial phagocytosis by neutrophils[41]. Although both the phagocytosis of bacteria by macrophages and efferocytosis are part of phagocytosis, the mechanisms are different. Inflammation usually enhances phagocytosis and the antimicrobial capacity of phagocytes in the short term, contributing to the clearance of pathogens. However, in cases of prolonged or chronic inflammation, phagocytosis may be inhibited and instead be detrimental to the clearance of pathogens. In addition, inflammation can indeed impair efferocytosis. This damage may be achieved through various mechanisms, including the adverse effects of inflammatory mediators, cellular metabolic disorders, and inflammation-induced cell death and tissue damage[24,46]. In the present study, we also found that LPS and IFN-γ stimulation resulted in impaired macrophage efferocytosis; however, overexpression of USP22 improved macrophage efferocytosis in inflammatory states, which may be partly attributed to the anti-inflammatory effect of USP22. In addition, it has been shown that oxidized lipoproteins can bind to efferocytosis-associated receptors and compete for the recognition of apoptotic cells, thereby inhibiting the phagocytosis of apoptotic cells by macrophages[22]. In this study, we likewise found that silencing USP22 promotes the uptake of oxidized lipoproteins, which may inhibit macrophage efferocytosis.

Interestingly, in this study, we found that USP22 promoted the expression of efferocytosis-associated receptors as well as bridging molecules and that this regulation is dependent on the activation of PPARγ. PPARγ is a member of the ligand-activated nuclear hormone receptor superfamily that strictly regulates the gene transcription of major efferocytosis-associated receptors[47,48]. Majai et al. demonstrated that the downregulation of PPARγ activity via the use of a small molecule inhibitor resulted in decreased phagocytosis of apoptotic neutrophils by human monocyte-derived macrophages due to the downregulation of several key efferocytosis-associated receptors, including CD36, AXL, TG2, and PTX3[25]. In addition, it has been shown that activated PPARγ enhances MERTK expression and promotes microglial phagocytosis in a mouse model of cerebral hemorrhage[49]. Although current studies have shown that PPARγ exerts insulin-sensitizing effects, the role of PPARγ in macrophages in cardiovascular diseases has been controversial[50]. Some studies have shown that macrophage PPARγ plays a protective role in atherosclerosis, but it has also been reported that PPARγ aggravates atherosclerosis by promoting foam cell formation[50,51]. More importantly, clinical trials using the PPARγ agonist rosiglitazone to treat patients with type 2 diabetes have not been successful because of increased myocardial infarction, heart failure, and cardiovascular mortality[52]. In light of this, our study focused on the upstream regulatory mechanisms of PPARγ, aiming to explore strategies that can both promote the positive effects of PPARγ and effectively curb the potential adverse effects triggered by its activation. In the present study, we found that USP22 regulates the stability of PPARγ through direct binding to PPARγ, which in turn enhances macrophage efferocytosis capacity, whereas USP22 inhibits foam cell formation. Consistent with previous findings, PPARγ is an important pathway for regulating macrophage efferocytosis in atherosclerosis, and SHP2 in macrophages acts as an anti-inflammatory agent and promotes efferocytosis by stabilizing PPARγ in atherosclerotic mice[53]. In addition, 5-aminolevulinic acid-mediated acoustic kinetic therapy promotes macrophage efferocytosis, cholesterol efflux, and anti-inflammatory responses by inducing foam cell apoptosis and thereby activating the PPARγ-LXRα-ABCA1/ABCG1 pathway, forming a beneficial cycle that contributes to the improvement of advanced plaques[54]. However, the exact role of PPARγ in human plaques has not yet been fully elucidated. Therefore, more studies are needed to determine the role and potential mechanisms of PPARγ in human plaques. In this study, we also found that USP22 regulates PPARγ stabilization through its deubiquitination function, which is consistent with previous findings in hepatocellular carcinoma cells[30]. However, USP22 does not seem to have a clear specificity in terms of its selectivity for PPARγ deubiquitination, and studies have reported that USP22 can deubiquitinate ATG5 and STING[21,40]. Whether USP22 affects immune response-associated other proteins related to the immune response

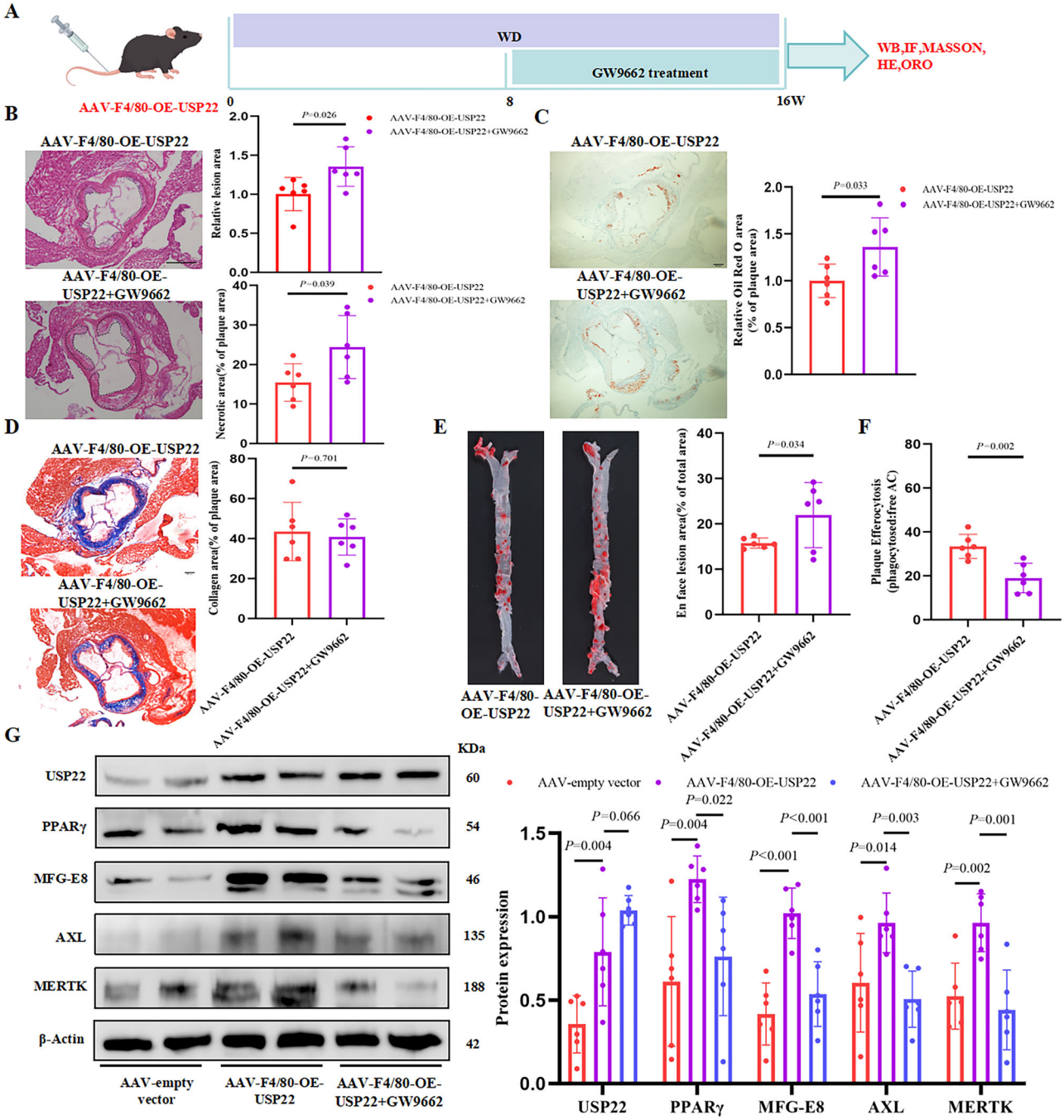

Fig. 6 | The protective effect of USP22 overexpression in macrophages against atherosclerosis is weakened by the GW9662. A In vivo experimental timeline. **B** Representative micrographs and quantification of H&E-stained aortic sinus cross-sectional sections are shown. Scale bar: 500 μm. **C** Representative micrographs and quantification of aortic sinus cross-sectional sections subjected to ORO staining are shown. Scale bar: 200 μm. **D** Representative micrographs and quantification of aortic sinus cross-sectional sections subjected to Masson staining are shown. Scale bar: 200 μm. **E** ApoE$^{-/-}$ mice were subjected to ORO staining of the aorta. **F** Quantification of lesion efferocytosis is shown. **G** Protein levels were measured by western blot. Each point is from a single mouse. *P* values are shown in the figure. Two-tailed unpaired *t*-test (**B**–**F**). One-way ANOVA (**G**). ($n = 6$).

is not yet fully understood and requires further study. Furthermore, we demonstrated that a USP22 inhibitor exacerbated atherosclerosis. Although no USP22-specific inhibitors are currently available for clinical treatment, and reports of cardiovascular events associated with USP22 inhibitors in basic experiments are lacking, our results suggest that we should consider the side effects of inhibiting the USP22 protein in the cardiovascular system.

The ApoE$^{-/-}$ mice given a WD are a well-characterized animal model of hyperlipidemia-induced atherosclerosis that mimics the progression of atherosclerosis in humans. Therefore, this study used ApoE$^{-/-}$ mice for modeling, and atherosclerotic plaques were observed in the arteries of the model group of mice, and large numbers of foam cells and unstructured necrotic material were seen in the aortic sinus, suggesting successful modeling[55,56]. We subsequently used adeno-associated virus overexpressing USP22 in macrophages to investigate its biological properties and found that USP22 could promote efferocytosis and stabilize plaques by regulating PPARγ. However, USP22 in macrophages has been shown to regulate

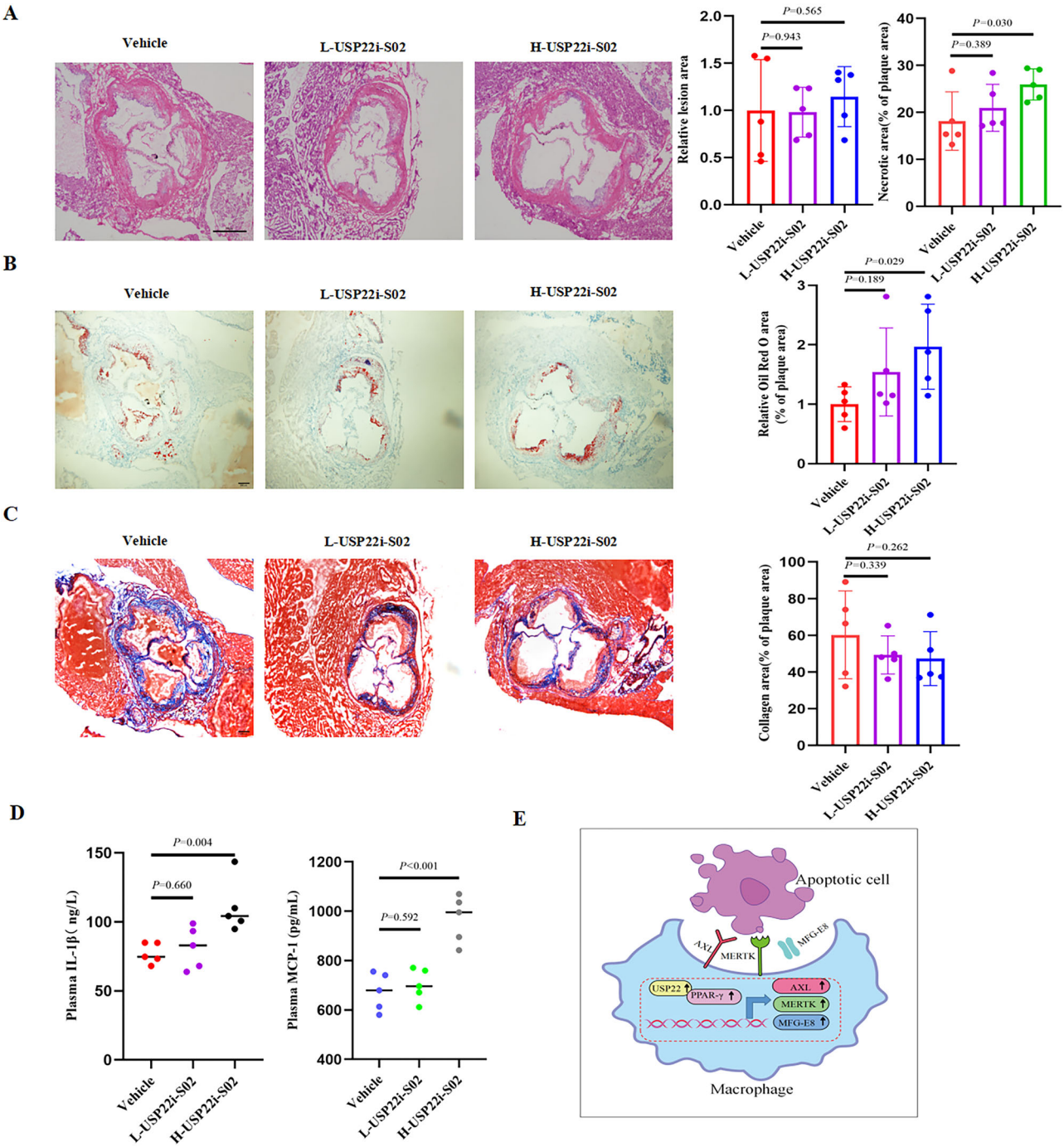

Fig. 7 | USP22 inhibitor exacerbates atherosclerosis in ApoE$^{-/-}$ mice. **A** Representative micrographs and quantification of H&E-stained aortic sinus cross-sectional sections are shown. Scale bar: 500 μm. **B**, **C** Representative micrographs and quantification of aortic sinus cross-sectional sections subjected to Masson and ORO staining are shown. Scale bar: 200 μm. **D** Plasma levels of MCP-1 and IL-1β in ApoE$^{-/-}$ mice are shown. Each point is from a single mouse. **E** In response to ACs stimulation, USP22 was elevated in the nucleus of macrophages, promoting efferocytosis-associated receptor and bridging molecule expression by stabilizing PPARγ, thereby improving plaque stability. *P* values are shown in the figure. One-way ANOVA (**A**–**D**). ($n = 5$).

NLRP3, and the role of NLRP3 in atherosclerosis in ApoE$^{-/-}$ mice is currently controversial. By superimposing NLRP3 defects on ApoE2 Ki mice, which are already susceptible to atherosclerosis, NLRP3 deficiency reduces the formation of atherosclerotic lesions in HFD-fed mice[57]. In addition, the use of lentivirus-mediated NLRP3 gene silencing or the selective NLRP3 inhibitor MCC950 slowed the progression of atherosclerotic plaques in ApoE$^{-/-}$ mice[58–60]. In contrast, however, Menu et al. showed no significant differences in plaque size or macrophage infiltration between ApoE$^{-/-}$ mice and ApoE$^{-/-}$ mice lacking NLRP3, ASC, or caspase-1[61]. A study have also reported unaltered atherosclerotic lesions after treatment with the selective NLRP3 inhibitor MCC950 in nondiabetic mice[62]. Possible explanations for this discrepancy have been hypothesized to be differences in atherogenic diet and hyperlipidemia levels, which may affect inflammatory responses and immune status. In addition to the time of modeling as well as the sex of the mice, which may have influenced the experimental results. Under the modeling conditions of this study, although we revealed the mechanism by which USP22 regulates efferocytosis-associated molecules through PPARγ, other possible regulatory pathways remain unexplored, and whether USP22

regulates NLRP3 and acts as an antiatherosclerotic agent through NLRP3 is not clear and needs to be further explored.

In the in vitro experiments of the present study, given the previous studies on macrophage efferocytosis and the fact that THP-1 cells are more morphologically and functionally characterized as similar to human primary monocytes[63–65], We used THP1-derived macrophages for validation. However, the differentiation process and functional properties of THP-1 cells may be affected by their cancerous background and may not fully mimic the physiological behaviors of primary macrophages. To better fit the atherosclerosis model, we also used primary mouse bone marrow macrophages for the experiments, and both came to the same conclusions. In the future, we can conduct experiments in human primary macrophages to verify whether the phenomenon observed in these experiment is generalizable. In addition, we cannot completely exclude the possible role of USP22 in other cell types in atherosclerosis in this study.

In conclusion, we showed that USP22 in macrophages promotes efferocytosis and alleviates the progression of atherosclerosis in $ApoE^{-/-}$ mice by regulating PPARγ. Targeting USP22 in macrophages may offer a promising approach to limit the progression of atherosclerotic lesions in patients at high risk for coronary heart disease.

Methods

Animals

$ApoE^{-/-}$ mice and C57BL/6 J mice were purchased from Beijing Viton Lever Co. Because of the protective effect of estrogen against atherosclerotic cardiovascular disease in females, in vivo studies of atherosclerosis were performed mainly in male $ApoE^{-/-}$ mice. An adeno-associated virus carrying the F4/80 promoter of macrophages and the flag-tagged USP22 gene (AAV-F4/80-OE-USP22) was injected into 7-week-old male $ApoE^{-/-}$ mice via the tail vein to overexpress USP22 in macrophages, and the AAV-empty vector was injected into the tail vein as a control. AAV-F4/80-OE-USP22 and the AAV-empty vector were provided by Hanbio (Shanghai, China). 8-week-old male $ApoE^{-/-}$ mice were fed a WD (HFHC, containing 40 kca% fat, 43 kca% carbohydrate and 17 kca% protein) for 16 weeks to establish an atherosclerosis model. All the animal experiments were performed in accordance with the Guidelines for the Care and Use of Laboratory Animals (NIH Publication, eighth edition, 2011) and were approved by the Animal Ethics Committee of the First Affiliated Hospital of Guangxi Medical University. The animals were euthanized via CO_2 inhalation followed by a second physical method, including cervical dislocation or decapitation.

Cell lines

THP-1 cells (human monocytic cell line) and Jurkat cells were purchased from Procell Biotechnology Co. (China, Wuhan). THP-1 cells and Jurkat cells were cultured in 1640 medium supplemented with 10% FBS and 1×penicillin/streptomycin. To generate a USP22- overexpressing THP-1 cell line (H-OE-USP22 THP-1), THP-1 cells were infected with packaged lentivirus carrying the human USP22 gene, while empty vector lentivirus-infected THP-1 cells were used as a control. The cells were subsequently selected with 0.25 μg/mL puromycin (Genomeditech) in a complete RPMI-1640 medium. THP-1 cells were induced to differentiate into macrophages by stimulation with 100 ng/mL phorbol-12-myristate-13-acetate (PMA) for 48 h. The lentiviruses were purchased from Shanghai Jiman Biotechnology Co.

BMDMs culture

BMDMs were isolated from 4 to 6-weeks-old male C57BL/6 mice and cultured in IMDM supplemented with 10% FBS and 20 ng/mL macrophage colony-stimulating factor (M-CSF, PeproTech, USA) for 7 days.

Apoptotic jurkat cells and apoptotic cell conditioned medium preparation

ACs were induced by intervention with 100 mM H_2O_2 in Jurkat cells for 0.5 h. The apoptosis rate of the Jurkat cells was >80%, as detected by flow cytometry. ACCM was prepared as previously described[66–68]. The ratio of ACs to macrophages was maintained at 5:1.

siRNA transfection

USP22 siRNA and the negative control were purchased from Hanbio (Shanghai, China) and used to transfect THP-1-derived macrophages and BMDMs in Opti-MEM via Lipo3000 according to the manufacturer's instructions. The target sequences used in this study are listed in Supplementary Table S4.

Total RNA extraction and RT-qPCR

Total RNA was extracted from the cells via Trizol. SYBR Green-based RT-qPCR was performed in a real-time PCR detection system (Bio-Rad). Relative mRNA expression was calculated via the $2^{-\Delta\Delta Ct}$ method. GAPDH was used as an internal control. The primer sequences are listed in Supplementary Table S5.

Nuclear and cytoplasmic protein extraction

Nuclear and cytoplasmic proteins were isolated via the Nuclear and Cytoplasmic Protein Extraction Kit (Solarbio, China) according to the manufacturer's protocol. The relevant information is listed in Supplementary Table S6.

Western blot

The following antibodies were used for western blot analyses: rabbit anti-USP22, rabbit anti-PPARγ, mouse anti-USP22, mouse anti-PPARγ, rabbit anti-AXL, rabbit anti-MERTK, rabbit anti-CD36, mouse anti-MFG-E8, rabbit anti-BCL-2, rabbit anti-BAX, rabbit anti-Ubiquitin, rabbit anti-LOX-1, rabbit anti-MSR1, rabbit anti-GAPDH, rabbit anti-H3 and rabbit anti-β-Actin. Antibody information is listed in Supplementary Table S7.

RNA-seq assay

THP-1-derived macrophages were treated with LPS (100 ng/mL) and IFN-γ (20 ng/mL) for 24 h. The treated cells were evaluated via an RNA-seq assay by Sangon Biotech (Shanghai, China). The sequencing data were then subjected to gene set enrichment analysis (GSEA) and the results were visualized.

Co-IP

The cell lysates were incubated with the appropriate antibody at 4 °C overnight. Then the samples were immunoprecipitated with protein A + G agar magnetic beads at 4 °C for 6 h. Subsequently, the immunoprecipitated samples were immunoblotted for coprecipitated protein detection.

Blood analysis

Mouse plasma HDL-C and LDL-C were measured according to the kit manufacturer's protocol (Jian Cheng Biologics, China). In addition, IL-1β and MCP-1 were quantified via an enzyme-linked immunosorbent assay (ELISA) kit.

Immunofluorescence

The following antibodies were used for immunofluorescence staining: rabbit anti-CD68, rabbit anti-F4/80, rabbit anti-USP22, rabbit anti-PPARγ and mouse anti-PPARγ.

In vitro apoptosis assay

Staining was performed via an Annexin V-FITC Apoptosis Detection Kit. The data were collected via a flow cytometer (BD, Biosciences) and analyzed via FlowJo software.

Foam cell formation assay

The macrophages were treated with 80 μg/mL oxidized low-density lipoprotein (ox-LDL) for 48 h and then stained with ORO to assess the intracellular lipid content. The ORO-positive area was measured with Image-Pro Plus 6.0 software.

DiI-ox-LDL uptake

THP-1-derived macrophages or BMDMs were incubated with 40 μg/mL DiI-ox-LDL for 4 h. DAPI staining was performed, and photographs were taken with an EVOS microscope and the data were quantified with Image-Pro Plus 6.0 software.

H&E, ORO, and Masson staining of aortic root sections

The aortic root sections were subjected to H&E, ORO, and Masson staining. H&E staining was used to determine the plaque area and percentage of the necrotic core area. ORO staining was used to determine the area of lipid deposition in the aortic plaques. Masson staining was used to determine the collagen fiber content of the aortic plaques. The samples were stained and photographed with a microscope, and the data were quantified via Image-Pro Plus 6.0 software.

In vitro efferocytosis assay

ACs labeled with CellTracker^{TM}CM-DiI^{+} were cocultured with macrophages at a ratio of 1:1 (ACs: macrophages) at 37 °C for 120 min to allow macrophages to phagocytose ACs. The macrophages were subsequently washed several times with precooled PBS to remove free AC and stained with F4/80 or CD68. Visualization and image capture of cells via EVOS microscopy. Efferocytosis index = double-positive cells/total F4/80-positive cells or CD68-positive cells × 100%.

To determine the efferocytosis capacity of THP-1-derived macrophages/BMDMs, ACs labeled with CellTracker^{TM}CM-DiI^{+} were cocultured with THP-1-derived macrophages labeled with CFSE or BMDMs at a ratio of 5:1 (ACs: macrophages) at 37 °C for 120 min, after which the macrophages were washed several times with precooled PBS to remove free ACs. BMDMs were stained with F4/80-FITC. The data were collected via BD flow cytometry and analyzed via FlowJo software. Efferocytosis index = double-positive cells/total F4/80-positive cells or CFSE-positive cells × 100%.

Lesion efferocytosis assay

The lesion efferocytosis assay was performed according to the previously described method[69,70]. Aortic root sections were double stained with TUNEL and CD68. The ratio of macrophage-associated TUNEL-positive cells to free TUNEL-positive cells was used to indicate the efferocytosis capacity.

Statistics and reproducibility

The data are expressed as the mean ± standard deviation (SD). Two-tailed unpaired *t*-test was used to compare differences between two groups. For comparisons involving more than two groups, one-way ANOVA was performed with LSD or Tukey or Tamhane's T2 multiple comparison test. Two-way ANOVA was used to assess significance for two groups with two variables. In vitro experiments included at least three biological replicates per group ($n \geq 3$), while in vivo experiments included at least five mice per group ($n \geq 5$). All the statistical analyses were performed via SPSS 13.0 for Windows software, and GraphPad Prism 8.0 software for graphs. P value < 0.05 was considered to indicate statistical significance.

Reporting summary

Further information on research design is available in the Nature Portfolio Reporting Summary linked to this article.

Data availability

The source data for the graphs analyzed in this study can be found in Supplementary data 2. Original blot images and FACS gate strategy are provided in the Supplementary Fig. S6 and Fig. S7. Other data will be made available from the corresponding author upon reasonable request.

Received: 20 November 2024; Accepted: 22 April 2025;
Published online: 29 April 2025

References

1. Wang, W. et al. Global Burden of Disease Study 2019 suggests that metabolic risk factors are the leading drivers of the burden of ischemic heart disease. *Cell Metab.* **33**, 1943–1956.e2 (2021).
2. Tsao, C. W. et al. Heart disease and stroke statistics—2022 update: a report from the American Heart Association. *Circulation* **145**, E9298–E9307 (2022).
3. Yurdagul, A., Doran, A. C., Cai, B., Fredman, G. & Tabas, I. A. Mechanisms and consequences of defective efferocytosis in atherosclerosis. *Front. Cardiovasc. Med.* **4**, 86 (2018).
4. Chistiakov, D. A., Melnichenko, A. A., Myasoedova, V. A., Grechko, A. V. & Orekhov, A. N. Mechanisms of foam cell formation in atherosclerosis. *J. Mol. Med.* **95**, 1153–1165 (2017).
5. Kunjathoor, V. V. et al. Scavenger receptors class A-I/II and CD36 are the principal receptors responsible for the uptake of modified low-density lipoprotein leading to lipid loading in macrophages. *J. Biol. Chem.* **277**, 49982–49988 (2002).
6. Zhang, H. et al. Augmenting ATG14 alleviates atherosclerosis and inhibits inflammation via promotion of autophagosome-lysosome fusion in macrophages. *Autophagy* **17**, 4218–4230 (2021).
7. Canfrán-Duque, A. et al. Macrophage-derived 25-hydroxycholesterol promotes vascular inflammation, atherogenesis, and lesion remodeling. *Circulation* **147**, 388–408 (2023).
8. Hu, X. et al. PTPN2 negatively regulates macrophage inflammation in atherosclerosis. *Aging* **13**, 2768–2779 (2021).
9. Kojima, Y., Weissman, I. L. & Leeper, N. J. The role of efferocytosis in atherosclerosis. *Circulation* **135**, 476–489 (2017).
10. Morioka, S., Maueröder, C. & Ravichandran, K. S. Living on the edge: efferocytosis at the interface of homeostasis and pathology. *Immunity* **50**, 1149–1162 (2019).
11. Cai, B. & Kasikara, C. TAM receptors and their ligand-mediated activation: role in atherosclerosis. In *Int. Rev. Cell Mol. Biol.* **357**, 21–33 (2020).
12. Tajbakhsh, A., Rezaee, M., Kovanen, P. T. & Sahebkar, A. Efferocytosis in atherosclerotic lesions: Malfunctioning regulatory pathways and control mechanisms. *Pharmacol. Ther.* **188**, 12–25 (2018).
13. Bhatia, V. K. et al. Complement C1q reduces early atherosclerosis in low-density lipoprotein receptor-deficient mice. *Am. J. Pathol.* **170**, 416–426 (2007).
14. Herrmann, J. et al. Increased ubiquitin immunoreactivity in unstable atherosclerotic plaques associated with acute coronary syndromes. *J. Am. Coll. Cardiol.* **40**, 1919–1927 (2002).
15. Wang, B., Cai, W., Ai, D., Zhang, X. & Yao, L. The role of deubiquitinases in vascular diseases. *J. Cardiovasc. Transl. Res.* **13**, 131–141 (2020).
16. Wang, B. et al. Disruption of USP9X in macrophages promotes foam cell formation and atherosclerosis. *J. Clin. Investig.* **132**, e154217 (2022).
17. Fu, Y. et al. USP14-mediated NLRC5 upregulation inhibits endothelial cell activation and inflammation in atherosclerosis. *Biochim. Biophys. Acta BBA - Mol. Cell Biol. Lipids* **1868**, 159258 (2023).
18. Gao, Q. et al. Abstract 2764: Ubiquitin-specific peptidase 22 controls integrin-dependent cancer cell stemness & metastasis. *Cancer Res.* **84**, 2764–2764 (2024).
19. Zhang, Z. et al. Ubiquitin-specific peptidase 22 promotes neural stem cells stemness maintenance and adult hippocampal neurogenesis, contributing to cognitive recovery following traumatic brain injury. *Neuroscience* **496**, 219–229 (2022).
20. Ma, S. et al. USP22 protects against myocardial ischemia–reperfusion injury via the SIRT1-p53/SLC7A11–dependent inhibition of ferroptosis-induced cardiomyocyte death. *Front. Physiol.* **11**, 551318 (2020).

21. Di, Q. et al. USP22 suppresses the NLRP3 inflammasome by degrading NLRP3 via ATG5-dependent autophagy. *Autophagy* **19**, 873–885 (2023).
22. Chang, M.-K. et al. Monoclonal antibodies against oxidized low-density lipoprotein bind to apoptotic cells and inhibit their phagocytosis by elicited macrophages: Evidence that oxidation-specific epitopes mediate macrophage recognition. *Proc. Natl. Acad. Sci.* **96**, 6353–6358 (1999).
23. Cai, S. et al. Mitochondrial dysfunction in macrophages promotes inflammation and suppresses repair after myocardial infarction. *J. Clin. Investig.* **133**, e159498 (2023).
24. Sharma, R. et al. Macrophage metabolic rewiring improves heme-suppressed efferocytosis and tissue damage in sickle cell disease. *Blood* **141**, 3091–3108 (2023).
25. Majai, G., Sarang, Z., Csomós, K., Zahuczky, G. & Fésüs, L. PPARγ-dependent regulation of human macrophages in phagocytosis of apoptotic cells. *Eur. J. Immunol.* **37**, 1343–1354 (2007).
26. Geng, Q. et al. PPARG-mediated autophagy activation alleviates inflammation in rheumatoid arthritis. *J. Autoimmun.* **146**, 103214 (2024).
27. Ye, G. et al. PPARα and PPARγ activation attenuates total free fatty acid and triglyceride accumulation in macrophages via the inhibition of Fatp1 expression. *Cell Death Dis.* **10**, 39 (2019).
28. Gao, Q. et al. Enhancing PPARγ by HDAC inhibition reduces foam cell formation and atherosclerosis in ApoE-deficient mice. *Pharmacol. Res.* **160**, 105059 (2020).
29. Zheng, S. et al. Yin-xing-tong-mai decoction attenuates atherosclerosis via activating PPARγ-LXRα-ABCA1/ABCG1 pathway. *Pharmacol. Res.* **169**, 105639 (2021).
30. Ning, Z. et al. USP22 regulates lipidome accumulation by stabilizing PPARγ in hepatocellular carcinoma. *Nat. Commun.* **13**, 2187 (2022).
31. Thorp, E. & Tabas, I. Mechanisms and consequences of efferocytosis in advanced atherosclerosis. *J. Leukoc. Biol.* **86**, 1089–1095 (2009).
32. Arandjelovic, S. & Ravichandran, K. S. Phagocytosis of apoptotic cells in homeostasis. *Nat. Immunol.* **16**, 907–917 (2015).
33. Elliott, M. R. & Ravichandran, K. S. The dynamics of apoptotic cell clearance. *Dev. Cell* **38**, 147–160 (2016).
34. Elliott, M. R., Koster, K. M. & Murphy, P. S. Efferocytosis signaling in the regulation of macrophage inflammatory responses. *J. Immunol.* **198**, 1387–1394 (2017).
35. Mehrotra, P. & Ravichandran, K. S. Drugging the efferocytosis process: Concepts and opportunities. *Nat. Rev. Drug Discov.* **21**, 601–620 (2022).
36. Jing, T. et al. Deubiquitination of the repressor E2F6 by USP22 facilitates AKT activation and tumor growth in hepatocellular carcinoma. *Cancer Lett.* **518**, 266–277 (2021).
37. Prokakis, E. et al. USP22 promotes HER2-driven mammary carcinoma aggressiveness by suppressing the unfolded protein response. *Oncogene* **40**, 4004–4018 (2021).
38. Doddapattar, P. et al. Myeloid cell PKM2 deletion enhances efferocytosis and reduces atherosclerosis. *Circ. Res.* **130**, 1289–1305 (2022).
39. Kong, P. et al. Inflammation and atherosclerosis: Signaling pathways and therapeutic intervention. *Signal Transduct. Target. Ther.* **7**, 131 (2022).
40. Karlowitz, R. et al. USP22 controls type III interferon signaling and SARS-CoV-2 infection through activation of STING. *Cell Death Dis.* **13**, 684 (2022).
41. Dietlein, N. et al. Usp22 is an intracellular regulator of systemic emergency hematopoiesis. *Sci. Immunol.* **7**, eabq2061 (2022).
42. Zhou, X.-X., Nie, H., Zhao, Y. & Tian, W. USP22 promotes vascular calcification via NF-κB signaling pathway. *Prog. Anat. Sci.* **28**, 125–128 (2022).
43. Montauti, E. et al. A deubiquitination module essential for Treg fitness in the tumor microenvironment. *Sci. Adv.* **8**, eabo4116 (2022).
44. Gennaro, V. J. et al. Control of CCND1 ubiquitylation by the catalytic SAGA subunit USP22 is essential for cell cycle progression through G1 in cancer cells. *Proc. Natl. Acad. Sci.* **115**, E9298–E9307 (2018).
45. Lin, Z. et al. USP22 antagonizes P53 transcriptional activation by deubiquitinating Sirt1 to suppress cell apoptosis and is required for mouse embryonic development. *Mol. Cell* **46**, 484–494 (2012).
46. Hosseini, Z. et al. Resolvin D1 enhances necroptotic cell clearance through promoting macrophage fatty acid oxidation and oxidative phosphorylation. *Arterioscler. Thromb. Vasc. Biol.* **41**, 1062–1075 (2021).
47. Luo, B. et al. Erythropoietin signaling in macrophages promotes dying cell clearance and immune tolerance. *Immunity* **44**, 287–302 (2016).
48. Croasdell, A. et al. PPARγ and the innate immune system mediate the resolution of inflammation. *PPAR Res.* **2015**, 549691 (2015).
49. Zheng, L. et al. Pentoxifylline alleviates ischemic white matter injury through up-regulating Mertk-mediated myelin clearance. *J. Neuroinflamm.* **19**, 128 (2022).
50. Chawla, A. Control of macrophage activation and function by PPARs. *Circ. Res.* **106**, 1559–1569 (2010).
51. Oppi, S. et al. Macrophage NCOR1 protects from atherosclerosis by repressing a pro-atherogenic PPARγ signature. *Eur. Heart J.* **41**, 995–1005 (2020).
52. Nissen, S. E. & Wolski, K. Effect of rosiglitazone on the risk of myocardial infarction and death from cardiovascular causes. *N. Engl. J. Med.* **356**, 2457–2471 (2007).
53. Wu, C. et al. Protein tyrosine phosphatase SHP2 in macrophages acts as an antiatherosclerotic regulator in mice. *Arterioscler. Thromb. Vasc. Biol.* **44**, 202–217 (2024).
54. Wang, H. et al. Sonodynamic therapy-induced foam cells apoptosis activates the phagocytic PPARγ-LXRα-ABCA1/ABCG1 pathway and promotes cholesterol efflux in advanced plaque. *Theranostics* **8**, 4969–4984 (2018).
55. Osada, J., Joven, J. & Maeda, N. The value of apolipoprotein E knockout mice for studying the effects of dietary fat and cholesterol on atherogenesis. *Curr. Opin. Lipidol.* **11**, 25–29 (2000).
56. Zadelaar, S. et al. Mouse models for atherosclerosis and pharmaceutical modifiers. *Arterioscler. Thromb. Vasc. Biol.* **27**, 1706–1721 (2007).
57. Abderrazak, A. et al. Anti-inflammatory and antiatherogenic effects of the NLRP3 inflammasome inhibitor arglabin in ApoE2.Ki mice fed a high-fat diet. *Circulation* **131**, 1061–1070 (2015).
58. Zheng, F., Xing, S., Gong, Z., Mu, W. & Xing, Q. Silence of NLRP3 suppresses atherosclerosis and stabilizes plaques in apolipoprotein E-deficient mice. *Mediators Inflamm.* **2014**, 507208 (2014).
59. Wang, R. et al. Activation of NLRP3 inflammasomes contributes to hyperhomocysteinemia-aggravated inflammation and atherosclerosis in apoE-deficient mice. *Lab. Investig.* **97**, 922–934 (2017).
60. Van Der Heijden, T. et al. NLRP3 inflammasome inhibition by MCC950 reduces atherosclerotic lesion development in apolipoprotein E–deficient mice—brief report. *Arterioscler. Thromb. Vasc. Biol.* **37**, 1457–1461 (2017).
61. Menu, P. et al. Atherosclerosis in ApoE-deficient mice progresses independently of the NLRP3 inflammasome. *Cell Death Dis.* **2**, e137–e137 (2011).
62. Sharma, A. et al. Specific NLRP3 inhibition protects against diabetes-associated atherosclerosis. *Diabetes* **70**, 772–787 (2021).
63. Bae, S.-H. et al. BMS794833 inhibits macrophage efferocytosis by directly binding to MERTK and inhibiting its activity. *Exp. Mol. Med.* **54**, 1450–1460 (2022).
64. Cao, D. et al. Macrophage angiotensin-converting enzyme reduces atherosclerosis by increasing peroxisome proliferator-activated receptor α and fundamentally changing lipid metabolism. *Cardiovasc. Res.* **119**, 1825–1841 (2023).

65. Chanput, W., Mes, J. J. & Wichers, H. J. THP-1 cell line: An in vitro cell model for immune modulation approach. *Int. Immunopharmacol.* **23**, 37–45 (2014).
66. Johann, A. M. et al. Apoptotic cell-derived sphingosine-1-phosphate promotes HuR-dependent cyclooxygenase-2 mRNA stabilization and protein expression. *J. Immunol.* **180**, 1239–1248 (2008).
67. Herr, B. et al. The supernatant of apoptotic cells causes transcriptional activation of hypoxia-inducible factor–1α in macrophages via sphingosine-1-phosphate and transforming growth factor-β. *Blood* **114**, 2140–2148 (2009).
68. Jin, G. et al. Tnfaip2 promotes atherogenesis by enhancing oxidative stress-induced inflammation. *Mol. Immunol.* **151**, 41–51 (2022).
69. Schlegel, M. et al. Silencing myeloid netrin-1 induces inflammation resolution and plaque regression. *Circ. Res.* **129**, 530–546 (2021).
70. Schrijvers, D. M., De Meyer, G. R. Y., Kockx, M. M., Herman, A. G. & Martinet, W. Phagocytosis of apoptotic cells by macrophages is impaired in atherosclerosis. *Arterioscler. Thromb. Vasc. Biol.* **25**, 1256–1261 (2005).

Acknowledgements

This project was supported by the Ministry of Finance of China and National Health and Family Planning Commission, the Guangxi Key Laboratory of Precision Medicine in Cardio-cerebrovascular Diseases Control and Prevention (22-035-18), Guangxi Clinical Research Center for Cardio-Cerebrovascular Diseases (AD17129014), Guangxi Science and technology planning project (Guike AB24010178), The central government guides local science and technology development funding projects (Guike ZY23055038), Guangxi Natural Science Youth Fund Project (2025GXNSFBA069008) and Young Leader Talent Training Program of Guangxi Medical University (202307). We also thank Figdraw (www.figdraw.com) for the assistance in creating Scheme.

Author contributions

Zhiyu Zeng, Feng Huang, and Senhu Tang designed this study; Senhu Tang, Chuanghong Lu, and Zhongyuan Meng performed experiments; Zihua Ye, Yue Qin, and Shenglin Xian collected and analyzed the data; Na Na performed text correction; Senhu Tang wrote the manuscript.

Competing interests

The authors declare no competing interests.

Ethical approval

All animal experiments were conducted in accordance with the Guide for the Care and Use of Laboratory Animals, and this study was approved by the Ethics Committee of the First Affiliated Hospital of Guangxi Medical University. We have complied with all relevant ethical regulations for animal use.

Additional information

Supplementary information The online version contains supplementary material available at https://doi.org/10.1038/s42003-025-08116-6.

Correspondence and requests for materials should be addressed to Feng Huang or Zhiyu Zeng.

Peer review information *Communications Biology* thanks Chunfu Zheng, Hosung Bae and the other, anonymous, reviewer(s) for their contribution to the peer review of this work. Primary Handling Editors: Dr Connie Wong and Dr Ophelia Bu.